Effects of Flame Configuration on Chemistry Tabulation

Shyam Menon[a], Runhua Zhao[b], Jagannath Jayachandran[b], Fokion N. Egolfopoulos[b]

[a]*Energy systems engineering, Oregon State University – Cascades, Bend, OR 97701*
[b]*Department of Aerospace and Mechanical Engineering*
University of Southern California, Los Angeles, California 90089-1453, USA

Abstract

Flamelet approaches utilizing tabulated chemistry are widely used in large eddy simulations of turbulent combustion. In this investigation, counterflow twin flames, counterflow reactants to products flames, as well as spherically expanding and imploding flames were utilized to assess the effect of choice of various stretched flame configurations on chemistry tabulation. The numerical simulations were carried out for methane/air flames at standard conditions using detailed description of chemical kinetics and molecular transport. Additionally, the effects of equivalence ratio, Lewis number, and reactant differential diffusion were investigated. Results showed that the H, OH, and CO mass fractions vary monotonically with stretch rate and could be used as tabulation parameters for the counterflow reactants to products and spherically expanding flames, but this is not the case for twin flames. Comparisons of the source terms of the progress variable in the three configurations revealed less than 3% differences at the location of peak reaction rate and 5-10% in the post-flame region at high stretch rates. On the other hand, differences in temperature predictions in the three configurations were found to be only 2-5%. Negatively stretched flames were determined to result in unique flamelet solutions that need to be incorporated into chemistry tabulations used in turbulent combustion. In ongoing work, this issue is further examined using results from direct numerical simulations of turbulent premixed methane-air flames.

1. Introduction

Flamelet approaches offer a computationally efficient methodology to simulate turbulent combustion phenomena. A central theme of these approaches is that a turbulent premixed flame can be viewed as an ensemble of steadily propagating strained flames wrinkled by the effect of the turbulent flow field [1]. The constituent strained flames maintain their reactive-diffusive structure even under the influence of intense wrinkling. The assumption is that this theory holds for Karlovitz numbers less than unity, which encompasses wrinkled and corrugated flamelets described in the Peters combustion regime diagram [2]. The validity of this theory for thin reaction zones and with Karlovitz numbers between 1 and 100 has been the subject of recent studies [3,4].

Once an ensemble of detailed solutions for the constituent flamelets is generated, the relevant quantities required for the numerical simulation such as chemical source terms, density, temperature, and species mass fractions are tabulated based on one or more parameters, which provide a unique mapping across the library of flamelet solutions. Transport equations for these parameters are then solved in the fluid dynamic simulation in addition to the usual conservation

equations. A variety of flamelet-type approaches of this kind can be found in the literature. These include the flamelet-generated manifolds (FGM) [5], flamelet prolongation of intrinsic low dimensional manifolds (FPI) [6], flamelet progress variable (FPV) approach [7], and level set methods [8].

In this regard, the choice of configuration used to generate the detailed solution for an individual flamelet could potentially have a strong impact on the solution. Flames incorporating stretch effects can be simulated using a number of different canonical configurations. Twin counterflow flames (CFF) that have reactants entering from both sides (T-F) or reactants on one side and hot products on the other side (R-to-P) generate stretch effects due to aerodynamic straining. Spherically expanding flames (SEF) produce positive stretch due to strain and curvature, while spherically imploding flames (SIF) generate negative stretch solely due to curvature [9].

The choice of optimal configuration to generate the flamelet library has received limited attention in previous studies. Nilsson and Bai [10] demonstrated that the T-F and R-to-P configurations yield very similar burning velocity predictions at low stretch rate, K, but the predictions diverge as K increases. Polifke et al. [11] showed that the imposed strain rate that leads to flame extinction, K_{ext}, is different in the two configurations. Hawkes and Chen [12] provided comparisons indicating that an R-to-P flamelet provides better agreement with strained laminar 2-D direct numerical simulation (DNS) data. It was observed also that turbulent flames were able to burn at K's higher than K_{ext}'s produced by T-F flames but within the extinction limits of R-to-P flames. Data extracted from the DNS results showed flames to be considerably influenced by negative stretch, with K's approaching magnitudes similar to those for positive stretch. It was noted also that the Lewis number (Le) for their computations was close to unity and suggested further work to confirm the findings for Le $\neq$ 1.0. Based partly on the observations of Hawkes and Chen [12], Kolla and Swaminathan [13] utilized also an R-to-P configuration to study turbulent V-flames and Bunsen flames. More recently, Knudsen et al. [3] showed that both T-F and R-to-P configurations provide similar results for large eddy simulation (LES) of a premixed turbulent jet flame. A further point worth noting is that the studies mentioned above considered solutions for steady strain. Hawkes and Chen [12] noted based on DNS that flamelets subjected to unsteady strain might exhibit quasi-steady behaviour.

While the observations mentioned above are worthwhile, no systematic study has been reported in which flamelet solutions obtained in different canonical configurations are compared. Furthermore, regardless of the configuration there is no consensus regarding the choice of the optimal parameters to tabulate the detailed flamelet solution. Aside from the progress variable, C, which maps the chemical states, variables such as elemental mass fractions (H, O, and N for a hydrogen/air flame) [6], CO mass fraction (Y_{CO}) [14], OH mass fraction (Y_{OH}) [15], temperature [16], and scalar dissipation rate of C [13] have been used to characterize the flamelet. In a recent study involving a methane (CH_4)-air mixture with an equivalence ratio ϕ = 0.7 and unburned mixture temperature T_u = 800 K, Knudsen et al. [3] utilized the H mass fraction (Y_H) as a tabulation parameter based on its monotonic behaviour. However, and as it will be discussed below, a non-

monotonic behaviour of Y_H with K has been observed by the authors using, similarly to Ref. 3, the T-F configuration but with T_u = 300 K.

In view of the aforementioned considerations, the main goal of this study was to assess the effects of flame configuration, choice of parameter, and non-equidiffusion on chemistry tabulation for CH_4–air flames. The first step of this work was to construct detailed solutions for CH_4/air mixtures with different ϕ and K using the various configurations. Non-equidiffusion effects were studied by modifying the Lennard-Jones (L-J) parameters of CH_4 to be that of hydrogen (H_2) with increased diffusivity and that of *n*-dodecane (n-$C_{12}H_{26}$) with reduced diffusivity. Next, the solutions were used to generate flamelets parameterized by C. Different tabulation parameters such as H/OH/CO mass fractions and temperature were investigated for their potential to be used as tabulation parameters to parameterize stretch effects. Flamelet libraries generated in this manner were compared using contour plots of different quantities such as source term of C, temperature, source term of CO, etc., in order to identify configuration dependent differences. Finally, a laminar reacting flow configuration was simulated using flamelet libraries derived from different configurations.

2. Modelling approach

CFFs (T-F and R-to-P) were simulated using a one-dimensional opposed-jet flow code [17,18] that integrates the conservation equations of mass, momentum, energy and species concentrations along the stagnation streamline. In the T-F configuration, the symmetry of the problem allows for the solution of only half the physical domain. In the R-to-P configuration, the temperature and composition of the products at the inlet of the burner is computed using an equilibrium calculation [19]. The velocities of the upper and lower jets in the R-to-P configuration were chosen to balance the momentum and establish the stagnation plane at the center of the computational domain. To capture the flame response at low K, a large separation distance (10 cm) was chosen to avoid heat loss to the inlet boundary. Grid independent solutions were achieved by using adaptive meshing method and confining the first and second gradients in the solutions. The reported K values correspond to the maximum absolute value of the axial velocity gradient in the hydrodynamic zone [18]. SEFs and SIFs were simulated using a recently developed transient one-dimensional reacting flow code (TORC) [20], using the Premix code [21] as framework. The conservation equations are integrated in spherical co-ordinates using a method of lines approach. An initial condition consisting of a stagnant pocket of hot burned gas is used to ignite the surrounding unburned mixture for SEFs while a premixed flame at a sufficiently large radius is used to initiate SIFs. K for SEFs and SIFs is equal to $(2/R_f)(dR_f/dt)$ (e.g. [20], where R_f is the instantaneous radius of the flame.

All codes were integrated with the CHEMKIN [22] and the Sandia transport [23] subroutine libraries. The H and H_2 diffusion coefficients of several key pairs are based on the recently updated set [24]. Mixture averaged formulation was utilized in all cases of the current study. The USC Mech II kinetic model [25] that consists of 111 species and 784 elementary reactions was reduced using the DRG method [26] to 24 species and 137 reactions. Both models were used to simulate

CFFs, while the reduced model was used in the SEF and SIF simulations that are computationally intensive. All simulations were carried out at 1 atm and T_u = 300 K.

Table 1. Effective Lewis number and ratio of fuel to oxygen diffusivities for various L-J parameters and equivalence ratios.

ϕ	Le_{eff}	D_{fuel}/D_{oxygen}
CH_4 L-J Parameters: Original Fuel Diffusivity		
0.7	0.99	1.14
1	1.03	1.16
1.4	1.09	1.17
n-$C_{12}H_{26}$ L-J Parameters: Decreased Fuel Diffusivity		
0.7	2.13	0.45
1	1.61	0.48
1.4	1.16	0.51
H_2 L-J Parameters: Increased Fuel Diffusivity		
0.7	0.76	1.67
1	0.93	1.67
1.4	1.12	1.68

The effects of differential diffusion were studied by varying the diffusivity of the fuel to mimic the behaviour of heavier and lighter fuels. Using a CH_4-air mixture as a baseline case, the Lennard-Jones (L-J) parameters of CH_4 were adjusted to reflect those of H_2 and *n*-$C_{12}H_{26}$ as was done by Jayachandran et al. [20]. The three cases are respectively referred to as 'original fuel diffusivity' (OFD), 'increased fuel diffusivity' (IFD), and 'decreased fuel diffusivity' (DFD). This modification allows for the isolation and study of non-equidiffusion effects keeping the chemistry the same and avoiding thus complications, for example, from fuel cracking if a heavier hydrocarbon had to be used. Table 1 lists the effective Lewis number (Le_{eff}) [27] and ratio of diffusivities to the mixture of fuel (D_{fuel}) and oxygen (D_{oxygen}) for different ϕ with the original and modified L-J parameters. Le_{eff} is defined as a weighted average of the fuel Lewis number, Le_F, and oxidizer Lewis number, Le_O. Le_{eff} becomes the average of Le_F and Le_O for a stoichiometric mixture while for an off-stoichiometric mixture *Le* of the deficient component is more heavily weighted [27].

3. Tabulation co-ordinate selection

The flamelet solutions were tabulated in a two-parameter space. One of the parameters is *C*, defined as $C = Y_{CO} + Y_{CO2} + Y_{H2} + Y_{H2O}$ [8,28]. A key requirement of the second mapping parameter is that its maximum (or minimum) value varies monotonically across the library of

flamelet solutions when plotted in C space, so that unique interpolations can be performed between solutions obtained for two different Ks. This is illustrated in Fig. 1 that depicts Y_H as a function of C for selected points on the S-curve generated for a CH_4-air flame at $\phi = 1.4$; note that Y_H is plotted on a log-scale. The Y_H profiles shift consistently downward resulting in the monotonic reduction of its maximum value ($Y_{H,max}$) which ensures a unique mapping. A second desirable feature is for the mapping parameter is to be as orthogonal as possible to C [29].

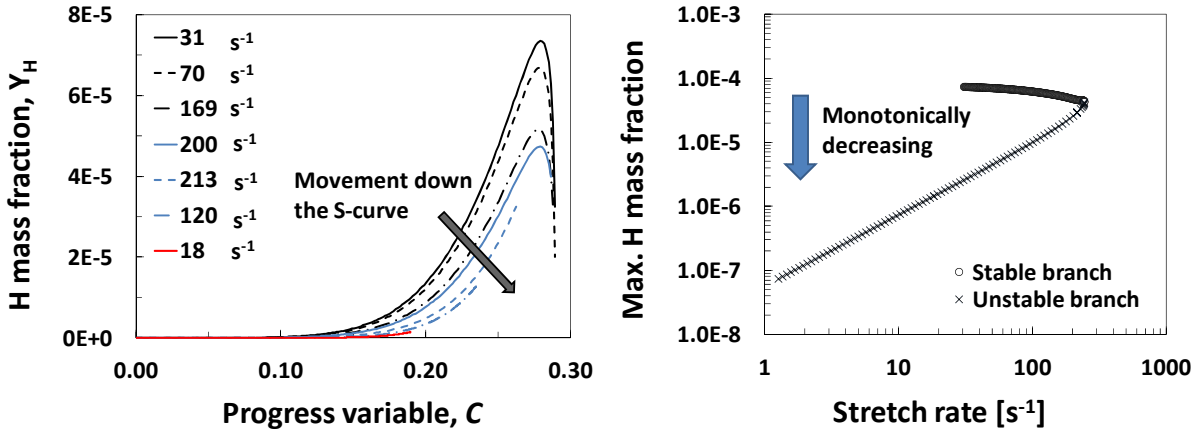

Figure 1. Y_H variation with C for different K using the T-F configuration for the $\phi = 1.4$ OFD case. The case with K of 213 s^{-1} lies to the left of the extinction point in the unstable branch. $Y_{H,max}$ plotted as a function of K shows monotonically decreasing behaviour.

The monotonicity of various parameters that can be used for chemistry tabulation of the flamelet solutions generated was investigated for the cases listed in Table 1 using T-F, R-to-P, SEF, and SIF configurations.

3.1 Twin-flame counterflow configuration

The variation of $Y_{H,max}$ with K is shown in Fig. 2 for 9 cases using the T-F configuration. Both $Y_{H,max}$ and K are plotted on log-scales. Monotonically decreasing behaviour is observed for 4 of the 9 cases. The results are lumped into three groups depending on the leading order effect. For all cases, $Y_{H,max}$ decreases monotonically in the unstable branch of the S-curve where the reduction in temperature has a leading order effect on chain branching.

For $\phi = 0.7$ and $\phi = 1.0$, $Le_{eff} > 1$ for the DFD case. Thus, with increasing K thermo-diffusive effects reduce the overall reactivity [30] resulting in a monotonically decreasing $Y_{H,max}$. For the same cases, (reactant) differential diffusion tends to make the mixture leaner locally, reducing further the reactivity and thus $Y_{H,max}$ [20,30]. For $\phi = 1.4$, $Le_{eff} > 1$ for the OFD and IFD cases and $Y_{H,max}$ decreases monotonically as well. In these cases, differential diffusion tends to make the mixture richer thus reducing its reactivity and $Y_{H,max}$.

For $\phi = 0.7$ and $\phi = 1.0$ with IFD, $Le_{eff} < 1$. In these cases, increasing K results in a corresponding increase in the reaction rate until reaching the extinction state. This response is further enhanced by differential diffusion that tends to make the mixture richer. A non-monotonic

behaviour is thus observed, with $Y_{H,max}$ increasing as the extinction state is approached followed by a decreasing trend within the unstable solution branch.

For $\phi = 0.7$ and $\phi = 1.0$ with OFD, $Le_{eff} \approx 1$. For these cases, as K increases, the flame approaches the stagnation plane. After the reaction zone reaches the stagnation plane, any further increase in stretch results in incomplete reaction due to insufficient residence time, causing thus increasing peak values of the H, OH, and fuel mass fractions prior to a sharp reduction at extinction. This phenomenon has been consistently observed in several fundamental investigations such as those performed by Dixon-Lewis [31] and Rogg [32]. Being a slow process, CO oxidation is particularly affected resulting in reduced temperatures and integrated heat release rates. These effects result in a non-monotonic behaviour for $Y_{H,max}$.

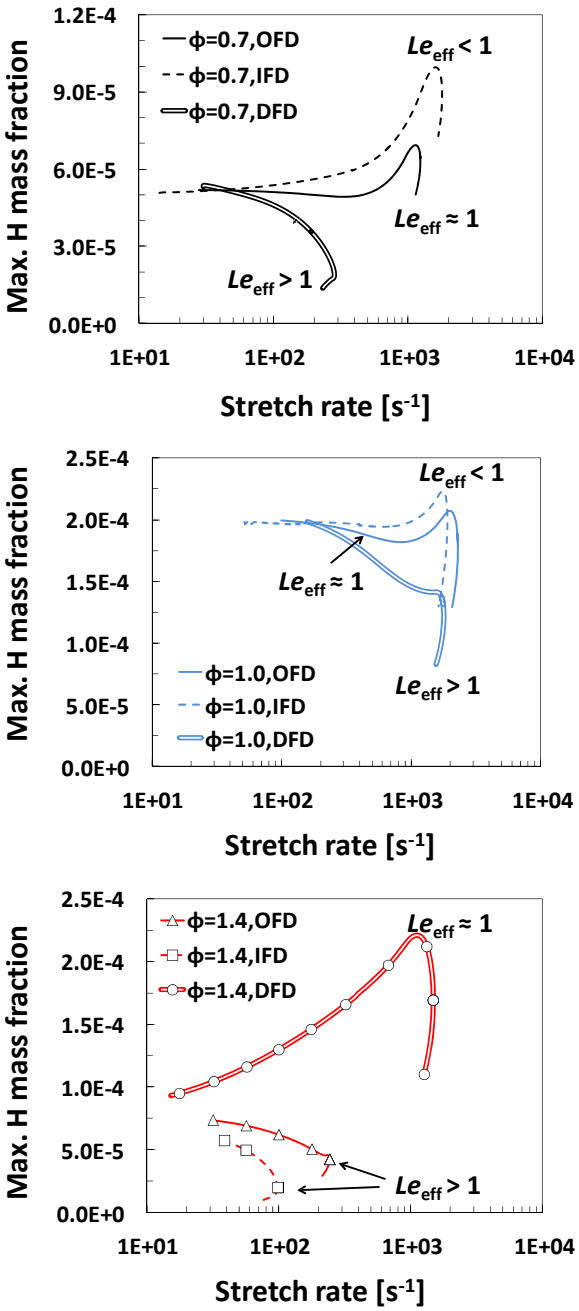

Figure 2. $Y_{H,max}$ variation with K for different ϕ and fuel diffusivities in the T-F configuration.

For $\phi = 1.4$ with DFD, a considerable increase in $Y_{H,max}$ is observed with increasing K prior to extinction. This is driven primarily by differential diffusion of oxygen into the reaction zone causing the mixture to become leaner locally. When the flame reaches the stagnation plane, differential diffusion effects are overshadowed by residence time, i.e. Damköhler number effects, which result in incomplete reaction and an overall non-monotonic behaviour for $Y_{H,max}$.

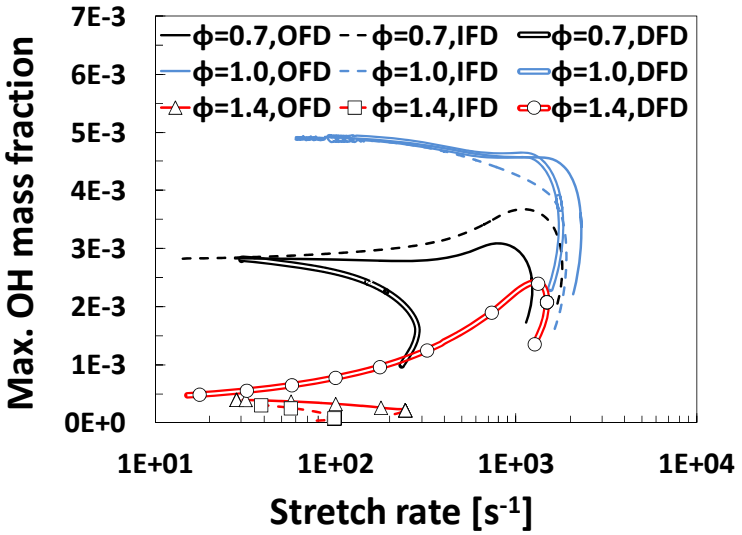

Figure 3. $Y_{OH,max}$ variation with K for different ϕ and fuel diffusivities in the T-F configuration.

Figure 3 depicts the variation of the maximum OH mass fraction ($Y_{OH,max}$) as a function of K. Monotonically decreasing behaviour is observed for 6 of the 9 cases. The reasons for the non-monotonic behaviour of $Y_{OH,max}$ are exactly the same as that mentioned in the previous section for $Y_{H,max}$. However, for the cases of ϕ = 1.0 with OFD and IFD, in which $Y_{H,max}$ exhibits non-monotonicity, $Y_{OH,max}$ varies monotonically with K. Analysis of the computed flame structures reveals that the main reactions contributing to the production and consumption of OH are the chain branching ($H + O_2 \rightarrow OH + O$) and the CO oxidation ($CO + OH \rightarrow CO_2 + H$) reactions respectively. With increasing K, the maximum temperature decreases monotonically causing a reduction in the reaction rate (peak and integrated) of both aforementioned reactions. Due to its higher activation energy, the chain branching reaction rate decreases faster than the CO oxidation reaction rate resulting in monotonically decreasing $Y_{OH,max}$. The same effect results in the non-monotonic behaviour of $Y_{H,max}$.

The response of the maximum CO mass fraction ($Y_{CO,max}$) to K is similar to $Y_{H,max}$ except for ϕ = 0.7 and ϕ = 1.0 with IFD for which $Y_{CO,max}$ increases monotonically. This is because the increasing reactivity with increasing K ($Le_{eff} < 1$) is followed by incomplete reaction as the flame approaches the stagnation plane with both contributing to a monotonically increasing $Y_{CO,max}$.

Figure 4 depicts the variation of the maximum temperature (T_{max}) as a function of K. Other than a slight increase prior to the extinction point for two cases (ϕ = 0.7 with IFD and ϕ = 1.4 with DFD), T_{max} decreases monotonically. The slight increase in T_{max} for ϕ = 0.7 with IFD ($Le_{eff} < 1$) can be attributed to Lewis number effects. The similar behaviour for ϕ = 1.4 with DFD is due to the progressive reduction of ϕ with K just upstream of the reaction zone due to differential diffusion as dictated by D_{fuel}/D_{oxygen} = 0.51 indicating the higher diffusion rate towards the reaction zone of O_2 compared to fuel [20]. These observations are consistent with the trends obtained for integrated heat release rates. Since temperature closely follows C, it is not always the best choice for the tabulation parameter [3]. However, neglecting a relatively low K range of two cases (ϕ = 0.7 with

IFD and $\phi = 1.4$ with DFD), it shows monotonic behaviour for all cases investigated here. As the flame reaches the stagnation plane and becomes restrained, residence time decreases leading to a drop in reaction rate and hence maximum temperature.

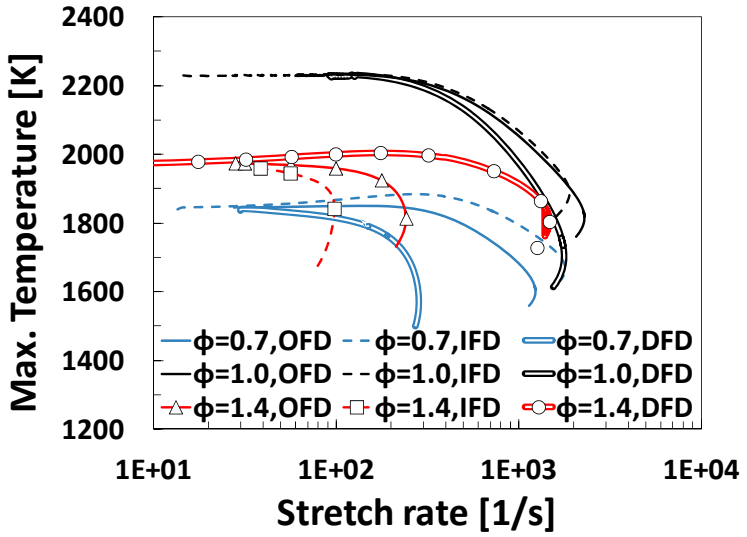

Figure 4. T_{max} variation with K for different ϕ and fuel diffusivities in the T-F configuration.

In summary, it was determined that for conditions under which increasing K weakens the mixture reactivity through Lewis number and differential diffusion effects, a monotonically decreasing behaviour is observed for $Y_{H,max}$ and $Y_{OH,max}$ making thus Y_H and Y_{OH} viable tabulation parameters. This is not the case though when non-monotonic behaviour is caused either by the reactivity being strengthened due to stretch effects or due to the flame merging at the stagnation plane resulting in incomplete reaction before extinction. In some cases this could be resolved by choosing $Y_{CO,max}$ as the tabulation parameter given that it increases both with increasing reactivity and incomplete reaction. Temperature is suitable for all cases. However, since it follows C closely, temperature profiles plotted as a function of C exhibit minor sensitivity to K making thus temperature an unsuitable tabulation parameter. In a practical LES it is possible to span a range of ϕ for a single operating condition [33]. In this case temperature might be the only viable parameter to characterize K variation since it monotonically decreases for all conditions.

3.2 Reactant-to-product counterflow configuration

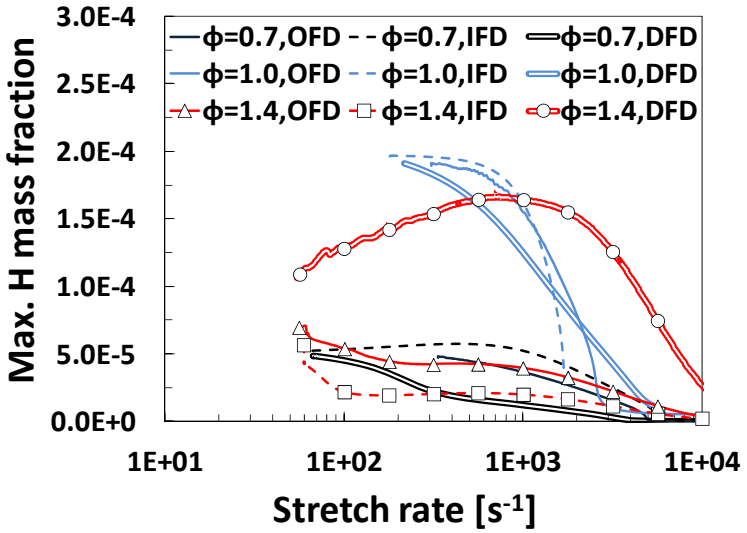

Figure 5. $Y_{H,max}$ variation with K for different ϕ and fuel diffusivities in the R-to-P configuration.

The variation of $Y_{H,max}$ with K in the R-to-P configuration is shown in Fig. 5, and a monotonic behaviour is seen for all but two cases ($\phi = 0.7$ with IFD and $\phi = 1.4$ with DFD). Due to the presence of high temperature equilibrium products downstream of the stagnation plane, as K increases abrupt extinction is not observed as in the T-F case, but instead a gradual transition occurs from a vigorous burning flame to a state in which a small but finite reactivity is sustained. At even higher K, this low reactivity region migrates on the product side and is sustained by the diffusive flux of reactants across the stagnation plane [34].

For $\phi = 1.4$ and DFD, the diffusion of O_2 makes the mixture locally leaner, increasing the reaction rate and $Y_{H,max}$ until the flame approaches the stagnation plane. For $\phi = 0.7$ with IFD, the differential diffusion effect is further aided by the thermo-diffusive effect given that $Le_{eff} < 1.0$, but only very minor non-monotonicity is observed.

For $\phi = 0.7$ and $\phi = 1.0$ with OFD, a monotonic behaviour is observed for $Y_{H,max}$ contrary to the T-F results. This is due to the ability of H and other species to diffuse into the product side driven by concentration gradients. Thus, with the R-to-P configuration, except for two cases, monotonic behaviour of $Y_{H,max}$ is observed and Y_H can be used as a tabulation parameter. Similar trends were observed also for Y_{OH} and Y_{CO}.

Temperature profiles show similar dependence to C as with the T-F configuration making it unsuitable as a tabulation parameter. Furthermore, in the case of the R-to-P flames the diffusion of heat from the burned gases across the stagnation plane raises the temperature profile on the reactant side and further reduces sensitivity of temperature profiles to variations in K. However, for the two cases ($\phi = 0.7$ with IFD and $\phi = 1.4$ with DFD) that Y_H and Y_{OH} show non-monotonic behaviour, temperature may be the only viable tabulation parameter.

3.3 Spherically expanding flame configuration

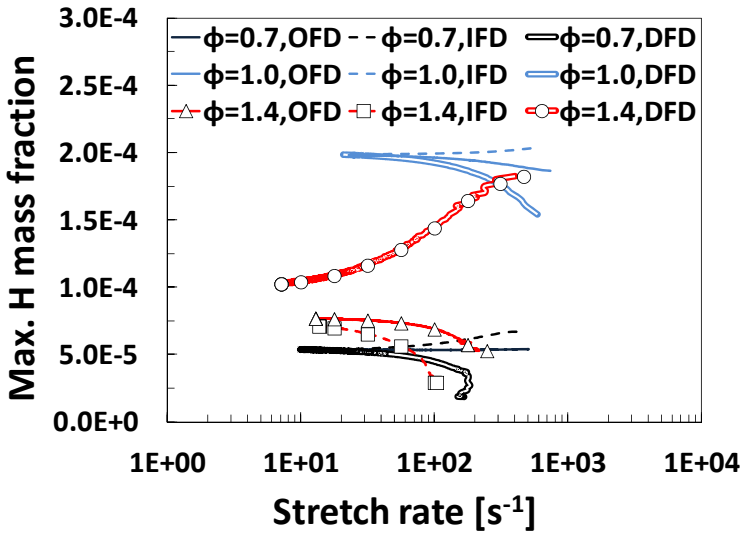

Figure 6. $Y_{H,max}$ variation with K for different ϕ and fuel diffusivities in the SEF configuration.

The variation of $Y_{H,max}$ with K in the SEF configuration is shown in Fig. 6, and either a monotonic increase or decrease is seen for all the cases. The trends are exactly the same as those seen in the T-F configuration for non near-extinction conditions. This makes SEF solutions amenable to tabulation using Y_H, Y_{OH}, or Y_{CO}. However, the need to initiate a SEF using an ignition kernel of small but finite radius implies that the maximum achievable K values are at least an order of magnitude smaller than those achievable using T-F and R-to-P flamelets. This could make SEF flamelets unsuitable for LES calculations that involve considerable stretching and possible local extinction of the flamelets.

3.4 Spherically imploding flame configuration

The variation of $Y_{H,max}$ with K in the SIF configuration is shown in Fig. 7 for $\phi = 0.7$ with OFD, IFD, and DFD. Results for negative stretch in Fig. 7 correspond to the SIF solutions while the results for positive stretch correspond to SEF solutions. The $Y_{H,max}$ profiles shown in Fig. 7 are in general continuous for $\phi = 0.7$ with IFD and DFD. However, the $\phi = 0.7$ case with OFD exhibits a change in slope going from positive to negative K. Such behaviour is consistent with changes in Markstein number during the transition from SEFs to SIFs observed by Ibareta et al. [35] and can be attributed to differences in Markstein numbers associated with strain and curvature [9,36]. However, a key result from the flamelet modelling perspective is presented in Fig. 8 which shows Y_H profiles as a function of C for selected solutions from SEFs and SIFs for $\phi = 0.7$ with IFD and DFD. Clearly, it can be seen that negative stretch produces distinct flamelet solutions that vary continuously from positive to zero to negative K. It is important to emphasize this point since in several previous LES investigations [3,13], negatively stretched flamelets have not been incorporated in the tabulation, and any negative stretch encountered in the simulation adopted a

solution corresponding to $K = 0$. For the $\phi = 0.7$ case whose solutions are plotted in Fig. 7-8, $Y_{H,max}$ varies monotonically across the range of solutions going from positive to negative K. However, non-monotonic behaviour was observed for $\phi = 1.0$ and $\phi = 1.4$. This requires additional consideration as regards incorporating the flamelets into the chemistry tabulation.

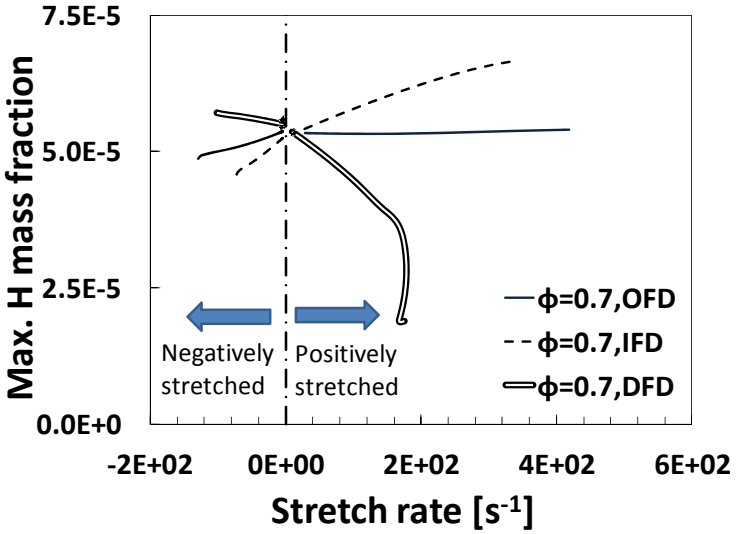

Figure 7. $Y_{H,max}$ variation with K for $\phi = 0.7$ and different fuel diffusivities in the SIF configuration.

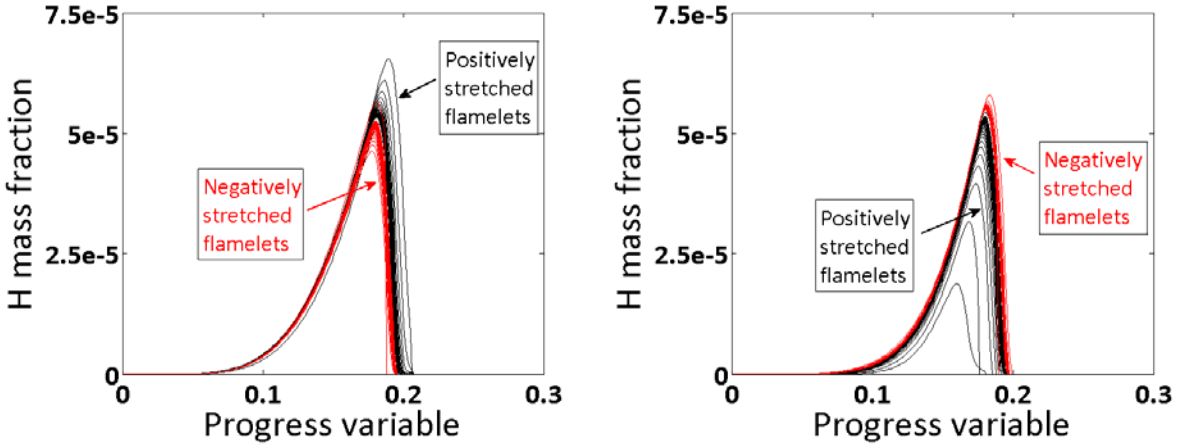

Figure 8. Y_H variation with C for solutions extracted from SEFs and SIFs. Solutions for $\phi = 0.7$ with IFD are plotted on the left and solutions for $\phi = 0.7$ with DFD are plotted on the right.

4. Comparing flame configurations

The coupling of chemistry to fluid dynamics in the tabulated chemistry approach is through the solution of the transport equation for C. In this equation, the source term of C ($\dot{\omega}_C$) has a leading order effect on laminar flame speed as well as on the fuel consumption and heat release rates. Hence, it is important to verify that the tabulated values of $\dot{\omega}_C$ are not configuration

dependent. Other parameters to consider are temperature and production rates of pollutants such as nitrous oxides (NO_x) and soot; NO_x and soot chemistry are not included in the kinetic model but conclusions can be drawn based on temperature. Only the configurations for positively stretched flames are considered in this analysis since no other negatively stretched flame solutions are as yet available to compare with the SIF solutions.

The configuration-dependent features associated with chemistry tabulation were assessed, by considering $\phi = 1.0$ and $\phi = 1.4$ flames with OFD in the T-F, R-to-P, and SEF configurations. For the $\phi = 0.7$ flame with OFD, no suitable parameter is available for tabulating the T-F solution. For all cases, the simulations were carried out using the reduced 24-species kinetic model so that the comparisons can focus on the configuration effects.

Furthermore, the tabulation parameters were Y_H and Y_{OH} for $\phi = 1.4$ and $\phi = 1.0$ respectively. The T-F solutions were considered as the baseline case and the differences on a percentage basis of each parameter was computed from the R-to-P and SEF configurations and presented in the form of contour plots in log scale.

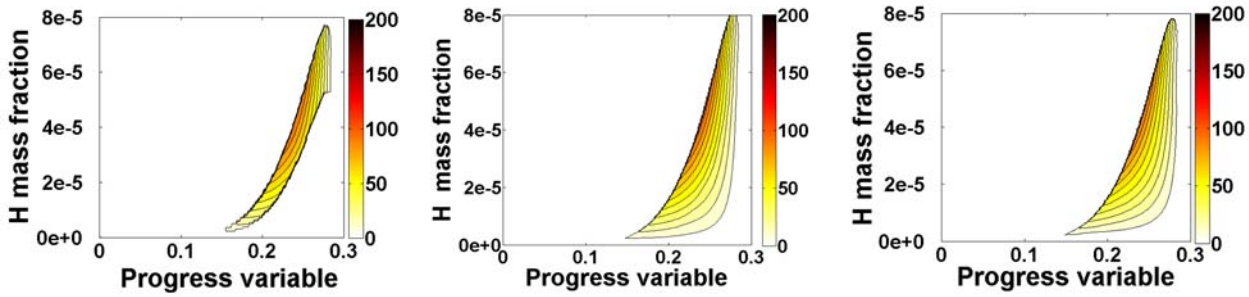

Figure 9. Contour plots of $\dot{\omega}_C$ plotted as a function of Y_H and C for the $\phi = 1.4$ OFD case. Left: SEF; Center: T-F; Right: R-to-P.

Figure 9 depicts contour plots of $\dot{\omega}_C$ as a function of C and Y_H for the three configurations with $\phi = 1.4$. The limited range of high K for the SEF configuration is reflected in the smaller area encompassed by the corresponding contour plot. The highest K for this case from the SEF configuration is 213 s^{-1}. The T-F and R-to-P configurations however, produce solutions that extend smoothly to very low but finite reaction rates and cover a larger area of the contour plot.

Figure 10 depicts contour plots of the percentage difference with respect to T-F in $\dot{\omega}_C$ for the SEF and R-to-P configurations with $\phi = 1.4$. The contours of the percentage difference are plotted on a log-scale. It is important to note not just the magnitude of differences between the configurations, but also the corresponding location in the flamelet where the differences occur. For this case, the peak values of $\dot{\omega}_C$ occur for $0.23 < C < 0.26$ and $2\text{x}10^{-5} < Y_H < 6\text{x}10^{-5}$. Any major differences in $\dot{\omega}_C$ in this region will have a leading order effect on the overall reactivity as mentioned earlier. The maximum differences observed in this region are of the order of less than 0.1%. Higher variation is observed in the oxidation region ($C > 0.27$) and at the lower edge of the contour surface that corresponds to high, near-extinction K ($Y_H < 10^{-5}$), but the source terms are also smaller in these regions. This behaviour was found not to depend on the second variable used for tabulation. For example, nearly identical results were obtained by using Y_{OH} for chemistry

tabulation instead of Y_H. Analysis showed a maximum of 2.5% difference in temperature between R-to-P and T-F and a 2% difference between SEF and T-F configurations, both being minor.

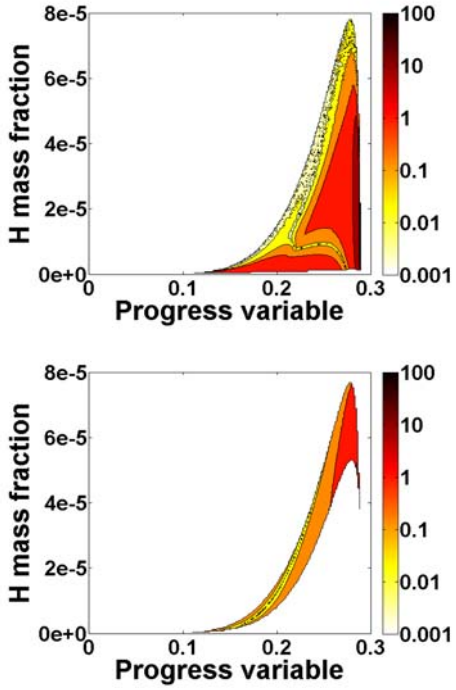

Figure 10. Contour plots of the percentage differences of $\dot{\omega}_C$ for the $\phi = 1.4$ OFD case in log scale. Bottom: SEF vs. T-F; Top: R-to-P vs. T-F.

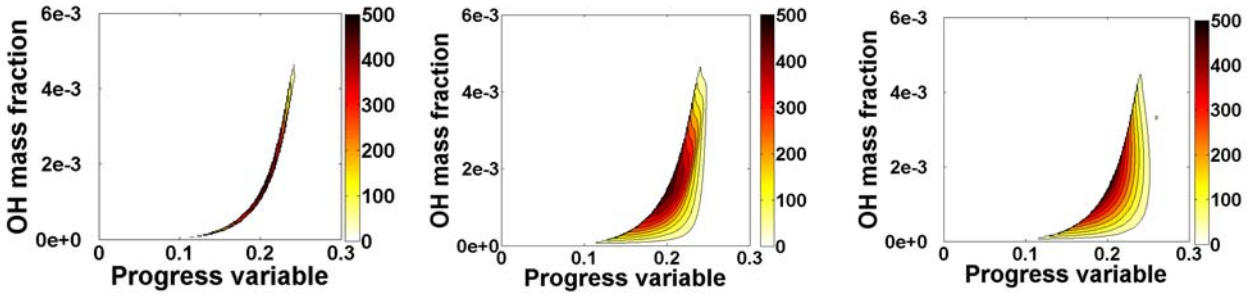

Figure 11. Contour plots of $\dot{\omega}_C$ plotted as a function of Y_{OH} and C for the $\phi = 1.0$ OFD case. Left: SEF; Center: T-F; Right: R-to-P.

Figure 11 depicts contour plots of $\dot{\omega}_C$ as a function of C and Y_{OH} for the three configurations with $\phi = 1.0$. A very small range of variation is obtained for Y_{OH} using the SEF configuration resulting in a narrow band of values in its contour plot. The highest K for this case from the SEF configuration is 737 s^{-1}. Again, the T-F and R-to-P configurations produce solutions that extend smoothly to very low but finite reaction rates.

Figure 12 depicts contour plots of the percentage difference with respect to T-F in $\dot{\omega}_C$ for the SEF and R-to-P configurations with $\phi = 1.0$. Larger differences compared to the T-F configuration can be seen compared to the previous case. The differences between the R-to-P and T-F configurations range from 1-3% in the peak reaction rate zone. Comparing temperatures,

maximum differences of 5% and 4% are obtained for the R-to-P and SEF configurations when compared to the T-F configuration.

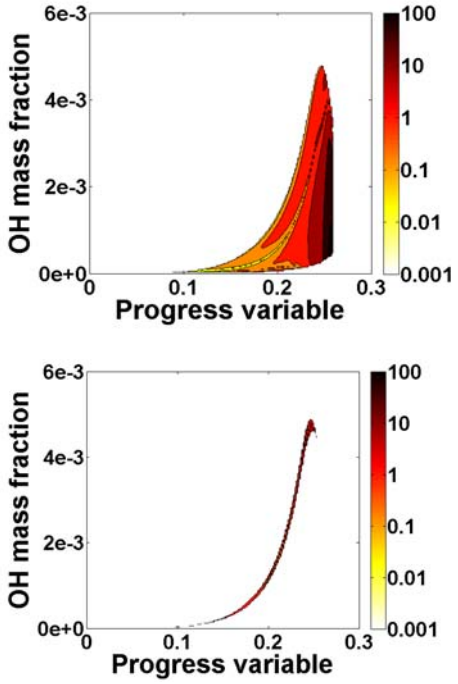

Figure 12. Contour plots of the percentage differences of $\dot{\omega}_C$ for the $\phi = 1.0$ OFD case in log scale. Bottom: SEF vs. T-F; Top: R-to-P vs. T-F.

Overall, the conclusion that can be drawn from comparing the source terms, $\dot{\omega}_C$ using the different flamelet configurations is that differences in the peak reaction zone are less than 3%. This implies that no significant differences in flame speed or heat release rate would be observed in LES studies that employ either configuration. The differences observed in the post-flame region could have some impact on the final gas temperature, and pollutant formation processes, which follow a slower timescale.

6. Concluding remarks

Detailed numerical simulations of counterflow twin flames, counterflow reactant-to-product flames, as well as spherically expanding and imploding flames were carried out in order to investigate the effects of each configuration on the tabulation of chemistry that is used in flamelet approaches in large eddy simulations. Methane/air mixtures at standard conditions were modelled, using detailed description of chemical kinetics and molecular transport. Additionally, the fuel diffusivity was varied significantly in order to assess effects associated with lighter and heavier fuels.

In past studies, the H mass fraction has been suggested as a tabulation parameter. However, in the present study it was determined that in twin flames its variation with stretch rate can be non-monotonic and thus it cannot be used as a universal tabulation parameter. Analysis showed that transport as well as kinetic effects for near-extinction conditions, cause this non-monotonic

behaviour. The variations of OH and CO mass fractions with stretch rate were found to be similar to H in most but not all cases. Temperature appears to be the only universal parameter capable of tabulating flamelet solutions using twin flames.

Reactant-to-product flames show a smooth transition from low to very high stretch rates due to the ability of the reaction zone to cross over to the product side thus eliminating near-extinction stagnation plane effects that cause non-monotonicity in twin flame solutions. Other than one case with a rich mixture and reduced diffusivity, reactant-to-product flames are amenable to tabulation using H/OH/CO mass fractions and are the ideal flamelets to use in LES computations utilizing tabulated chemistry. The same can be said about spherically expanding flames except for the fact that these flames cannot achieve high stretch rates unlike the other two configurations due to ignition effects. This limits the capability of spherically expanding flames to be used for simulations involving high stretch rates and local extinction.

Spherically imploding flame solutions provide flamelets corresponding to negative stretch. Results combining flamelet solutions from spherically expanding and imploding flames show a continuous variation going from positive to zero to negative stretch. Thus, negatively stretched flamelets should not be approximated by a zero stretch flamelet. This emphasizes the need to incorporate negatively stretch flamelets into tabulations used in large eddy simulations where it is likely to occur as demonstrated by previous detailed numerical simulations of turbulent flames.

The values of the source term of the progress variable as determined in the three positively stretched configurations were compared for stoichiometric and rich flames. Differences of less than 3% at the peak reaction rate location and of the order of 5-10% in the post-flame region were identified. The differences in predicted temperatures were smaller, of the order of 2-5%.

While the observed differences between the various flamelet configurations in the present investigation are relatively small, the conditions of each problem solved by LES need to be critically evaluated to assess potentially larger effects based on a variety of conditions and the effects of negative stretch that does not seem to be accounted for at present. It is recommended also that negatively stretched flamelets are incorporated in the tabulation by considering a number of configurations as is the case for positively stretched flamelets.

7. Future work

In order to further elucidate the role of configuration dependent features on chemistry tabulation, DNS simulation results of turbulent premixed methane/air flames have been obtained from work performed by Lapointe et al. [37]. These simulations are performed for $\phi = 0.9$, initial pressure of 1 atm and unburned temperature of 300 K. The Karlovitz number for these simulations is about 200. The data is currently being post-processed with an aim of obtaining joint probability density functions (PDF's) of fuel consumption rate and source term of the progress variable as a function of temperature. These joint PDF's will be overlaid with solutions of strained flamelets from different configurations. Further, the temperature and species distributions across various flame cross-sections through the DNS simulation domain will be compared with 1-D flamelets from

different configurations having similar strain rates. These analyses will hopefully shed some light on configuration dependent effects on chemistry tabulation.

Acknowledgements

This material is based upon work supported as part of the CEFRC, an Energy Frontier Research Center funded by the U.S. Department of Energy, Office of Science, and Office of Basic Energy Sciences under Award Number DE-SC0001198.

References

1. K.N.C. Bray, *Turbulent flows with premixed reactants*, in *Turbulent Reacting Flows*, P.A. Libby and F.A. Williams, eds., Springer-Verlag, Berlin, 1980, pp. 115–183.
2. N. Peters, *The turbulent burning velocity for large-scale and small-scale turbulence*, J. Fluid Mech. 384 (1999), pp. 107–132.
3. E. Knudsen, H. Kolla, E.R. Hawkes, and H. Pitsch, *LES of a premixed jet flame DNS using a strained flamelet model*, Combust. Flame 160 (2013), pp. 2911-2927.
4. F.T.C. Yuen and O.L. Gulder, *Turbulent premixed flame front dynamics and implications for limits of flamelet hypothesis*, Proc. Combust. Inst. 34 (2013), pp. 1393-1400.
5. J.A. van Oijen, F.A. Lammers, and L.P.H. de Goey, *Modeling of complex premixed burner systems by using flamelet-generated manifolds*, Combust. Flame 127 (2001), pp. 2124-2134.
6. O. Gicquel, N. Darabiha, and D. Thevenin, *Laminar premixed hydrogen/air counterflow flame simulations using flame prolongation of ILDM with differential diffusion*, Proc. Combust. Inst. 28 (2000), pp. 1901-1907.
7. C.D. Pierce and P. Moin, *Progress-variable approach for large-eddy simulation of non-premixed turbulent combustio*n, J. Fluid. Mech. 504 (2004), pp. 73-97.
8. E. Knudsen and H. Pitsch, *A dynamic model for the turbulent burning velocity for large eddy simulation of premixed combustion*, Combust. Flame 154 (2008), pp. 740-760.
9. D. Bradley, P.H. Gaskell, and X.J. Gu, *Burning velocities, Markstein lengths, and flame quenching for spherical methane-air flames: a computational study*, Combust. Flame 104 (1996), pp. 176-198.
10. P. Nilsson and X.S. Bai, *Effects of flame stretch and wrinkling on co formation in turbulent premixed combustion*, Proc. Combust. Inst. 29 (2002), pp. 1873-1879.
11. W. Polifke, P. Flohr, and M. Brandt, *Modeling of inhomogeneously premixed combustion with an extended TFC model*, J. Eng. Gas Turbines Power 124 (2002), pp. 58-65.
12. E.R. Hawkes and J.H. Chen, *Comparison of direct numerical simulation of lean premixed methane–air flames with strained laminar flame calculations*, Combust. Flame 144 (2006), pp. 112-125.
13. H. Kolla and N. Swaminathan, *Strained flamelets for turbulent premixed flames, I: Formulation and planar flame results*, Combust. Flame 157 (2010), pp. 943-954.
14. J.A. van Oijen and L.P.H de Goey, *Modelling of premixed counterflow flames using the flamelet-generated manifold method*, Combust. Theor. Model. 6 (2002), pp. 463-478.

15. J.A. van Oijen, R.J.M. Bastiaans, and L.P.H. de Goey, *Low-dimensional manifolds in direct numerical simulations of premixed turbulent flames*, Proc. Combust. Inst. 31 (2007), pp. 1377-1384.
16. A.W. Vreman, J.A. van Oijen, L.P.H de Goey, and R.J.M. Bastiaans, *Direct numerical simulation of hydrogen addition in turbulent premixed Bunsen flames using flamelet-generated manifold reduction*, Int. J. Hydrogen Energ. 34 (2009), pp. 2778-2788.
17. R.J. Kee, J.A. Miller, G.H. Evans, and G. Dixon-Lewis, *A computational model of the structure and extinction of strained, opposed flow, premixed methane-air flames*, Proc. Combust. Inst. 22 (1989), pp. 1479-1494.
18. F.N. Egolfopoulos and C.S. Campbell, *Unsteady counterflowing strained diffusion flames: diffusion-limited frequency response*, J. Fluid Mech. 318 (1996), pp. 1-29.
19. A.E. Lutz, R.J. Kee, and J.A. Miller, *Equil: A program for computing chemical equilibria*, Tech. Rep., Sandia National Laboratories, Livermore, California, USA, 1996.
20. J. Jayachandran, R. Zhao, and F.N. Egolfopoulos, *Determination of laminar flame speeds using stagnation and spherically expanding flames: Molecular transport and radiation effects*, Combust. Flame 161 (2014), pp. 2305-2316.
21. R.J. Kee, J.F. Grear, M.D. Smooke, and J.A. Miller, *Premix: A FORTRAN program for modeling laminar one-dimensional premixed flames*, Tech. Rep. SAND85-8240, Sandia National Laboratories, Livermore, California, USA, 1985.
22. R.J. Kee, F.M. Rupley, and J.A. Miller, *Chemkin II: A FORTRAN chemical kinetics package for the analysis of gas-phase chemical kinetics*, Tech. Rep. SAND89-8009, Sandia National Laboratories, Livermore, California, USA, 1989.
23. R.J. Kee, J. Warnatz, and J.A. Miller, *A FORTRAN computer code package for the evaluation of gas-phase viscosities*, Tech. Rep. SAND83-8209, Sandia National Laboratories, Livermore, California, USA 1983.
24. Y. Dong, A. T. Holley, M.G. Andac, F.N. Egolfopoulos, S.G. Davis, P. Middha, and H. Wang, *Extinction of premixed H_2/air flames: Chemical kinetics and molecular diffusion effects*, Combust. Flame 142 (2005), pp. 374–387.
25. H. Wang, X. You, A. V. Joshi, Scott G. Davis, A. Laskin, F.N. Egolfopoulos, and C. K. Law, *USC-Mech Version II. High-Temperature Combustion Reaction Model of H2/CO/C1-C4 Compounds*, available at http://ignis.usc.edu/USC_Mech_II.htm (accessed 16th December 2014).
26. T. Lu and C.K. Law, *A directed relation graph method for mechanism reduction*, Proc. Combust. Inst. 30 (2005), pp. 1333–1341.
27. M. Matalon, *Flame dynamics*, Proc. Combust. Inst. 32 (2009), pp. 57-82.
28. M. Ihme and H. Pitsch, *Prediction of extinction and reignition in nonpremixed turbulent flames using a flamelet/progress variable model: 2. Application in LES of Sandia flames D and E*, Combust. Flame 155 (2008), pp. 90-107.
29. M. Ihme, L. Shunn, and J. Zhang, *Regularization of reaction progress variable for application to flamelet-based combustion models*, J. Comp. Phys. 231 (2012), pp. 7715-7721.
30. C.K. Law, *Combustion Physics*, Cambridge University Press, New York, USA, 2006, p. 411.
31. G. Dixon-Lewis, *Structure of laminar flames*, Proc. Combust. Inst. 23 (1991), pp. 305-324.
32. B. Rogg, *Response and flamelet structure of stretched premixed methane-air flames*, Combust. Flame 73 (1988), pp. 45-65.

33. B. Fiorina, O. Gicquel, L. Vervisch, S. Carpentier, and N. Darabiha, *Premixed turbulent combustion modeling using tabulated detailed chemistry and PDF*, Proc. Combust. Inst. 30 (2005), pp. 867-874.
34. P.A. Libby and F.A. Williams, *Structure of laminar flamelets in premixed turbulent flames*, Combust. Flame 44 (1982), pp. 287-303.
35. A.F. Ibarreta, J.F. Driscoll, and D.A. Feikema, *Markstein numbers of negatively stretched premixed flames: Microgravity measurements and computations*, Proc. Combust. Inst. 29 (2002), pp. 1435-1443.
36. P. Clavin and J.C. Grana-Otero, *Curved and stretched flames: the two Markstein numbers*, J. Fluid Mech. 686 (2011), pp. 187-217.
37. Lapointe, S., Blanquart, G., *Private communication*.